

**One-way diffraction effects in photonic crystal gratings made of isotropic materials**

Andriy E. Serebryannikov\*

*Technische Universitaet Hamburg-Harburg, D-21071 Hamburg, Germany*

(Received 30 December 2008; revised manuscript received 25 July 2009; published 8 October 2009)

The anomalous diffraction effects arising in the intrinsically isotropic photonic crystal gratings with different periods of the front-side and back-side interfaces are studied with the emphasis put on wideband one-way transmission. It is demonstrated that more than 80 percent of the incident-wave energy can be transmitted unidirectionally, i.e., with zero transmission in the opposite direction, by changing side of illumination only, while polarization always remains linear. Most but not all of the related diffraction effects can be predicted using isofrequency contours (IFCs) and wave-vector diagrams, which take into account the IFC-shape-dependent additional transmission channels that can appear due to corrugations. Three main regimes, i.e., isolation and bidirectional and unidirectional translation, can be distinguished, depending on whether the front-side corrugations affect the far field in the half space bounded by the back-side interface, and whether transmission is vanishing only at illumination from the side of one of the interfaces. The conditions providing the existence of these regimes are given and discussed in terms of the features of wave-vector diagrams. In some cases, similar regimes can appear being in contradiction with these conditions. Variation in the angle of incidence and the angle between the characteristic directions of photonic crystal and the interfaces of the corresponding noncorrugated structure allows one extending variety of situations, in which unidirectional transmission can be realized. The general condition of unidirectionality is that the zero diffraction order is not coupled to a Floquet-Bloch wave.

DOI: [10.1103/PhysRevB.80.155117](https://doi.org/10.1103/PhysRevB.80.155117)

PACS number(s): 42.70.Qs, 42.25.Fx, 42.25.Bs, 78.20.Ci

**I. INTRODUCTION**

The impressive progress has occurred during the past two decades in theory and applications of photonic crystals (PCs), which show a unique potential in controlling light propagation. Among others, PCs with curvilinear virtual interfaces became a focus of interest, promising useful extensions of the known frequency and directional selectivity regimes. Curvilinearity in PCs with conventional linear lattices has been used in planoconcave lenses,<sup>1–3</sup> mirrors,<sup>4</sup> and dual-lattice splitters.<sup>5</sup> Another class of curvilinear PCs is characterized by that not only the interface but also lattice itself is curvilinear. For example, it is worth mentioning coaxial PCs,<sup>6</sup> single-layer atoll, or corall optical resonators,<sup>7,8</sup> and one-dimensional circular optical resonators.<sup>9</sup> The topologically similar but multilayer structures have been recently proposed for the use as invisibility cloaks.<sup>10–12</sup>

Linear-lattice PCs with corrugated surface layer(s) and defect-mode waveguide have been suggested for obtaining the beaming effect, which dominant physics includes the existence of the surface waves arising due to corrugations.<sup>13–16</sup> Similar effect can appear in PCs with coupled defect-mode cavities located in a subsurface layer, which can be considered as an inner gratinglike corrugation.<sup>17</sup> In Ref. 18, the effect of periodic corrugations, which are introduced on one of the interfaces, has been studied for a dual-lattice PC with the emphasis on stealth applications. A variety of anomalous transmission effects can exist in finite-thickness pieces of two-dimensional dielectric and metallic PCs with one-side deep gratinglike corrugations (PC gratings).<sup>19</sup> In particular, nonordinary opaque ranges (ORs) of transmission<sup>20</sup> have been demonstrated, within which some formally propagating diffraction orders are suppressed. The wavelength values, at which individual diffraction orders start contributing to the

transmission, can be shifted in the PC gratings as compared to the corresponding Rayleigh wavelengths, and furthermore can change their conventional order.<sup>19</sup> On the other hand, corrugation of the initially smooth, totally reflecting, virtual interface of a PC can provide a coupling to an otherwise uncoupled Floquet-Bloch (FB) wave. For an one-dimensional PC, introducing a corrugated surface layer has been used as an alternative route for obtaining negative refraction.<sup>21</sup>

One of the basic effects related to the nonordinary ORs in two-dimensional PC gratings manifests itself in that some higher orders can show one-way (unidirectional) transmission. This effect has been observed but not studied in detail in Ref. 19. Contrary to the branched-slit metallic gratings from Ref. 22, in which one-way transmission can also occur, it can be a wideband effect for PC gratings. The common feature of the gratings in Refs. 19 and 21 is that they are nonsymmetric, i.e., show different periods of the front- and back-side interfaces. It can be expected that if the zero order, which is responsible for reciprocal transmission, is not coupled to a FB wave, the situation can be realizable in these structures when transmission substantially differs for illumination from the side of one of the grating interfaces and that from the opposite side. In turn, reflection in these two cases should differ significantly. It is noteworthy that one-way transmission effects are obtained in Refs. 19 and 22 without using anisotropic constituents. This is distinguished from the conventional way, which is realized, for example, in gyromagnetic and gyroelectric crystals containing anisotropic constituents.<sup>23–26</sup>

Diffraction on relief gratings, which represent a periodically corrugated boundary between an air half space and a homogeneous negative-index half space has been studied in Refs. 27–29. Anomalous transmission effects, some of which being similar to those in Ref. 19, can appear in finite-

thickness gratings made of a zero-permittivity material.<sup>30</sup> For nonzero-index materials, the similarity in dispersion features of a homogeneous material and a FB wave in a PC often occurs so that the corresponding performances are associated with either metamaterials or dispersive plasmonic and polaritonic materials. Therefore, it is reasonable expecting that the effects observed in Refs. 27–30 might have analogs in PC gratings and vice versa.

It is also worth noting a variety of the interesting physical effects arising in the combined structures, which contain a surface-relief grating and a volume grating.<sup>31–33</sup> Surface gratings can demonstrate scattering into nonspecular orders and, hence, rechannel the incident energy while the used volume gratings are characterized by specular scattering only but show peculiar distinctive features in transmission and reflection. A stack of a PC containing a linear-defect waveguide with a finite-thickness dielectric grating,<sup>34</sup> which has been used to couple an otherwise uncoupled defect mode to the outer space, is similar in some sense to the above mentioned combined structures. In the contrast, our PCs gratings themselves combine the features of the both surface and volume gratings. In fact, they represent the structured gratings, whose unusual diffraction features are determined by the simultaneous contribution of the effects typical for conventional (noncorrugated) PCs and those for conventional diffraction gratings.

In this paper, the anomalous diffraction effects in two-dimensional PC gratings with one- and two-side corrugations will be studied with the emphasis put on one-way transmission effects and the peculiarities of using dispersion results to predict them. It will be shown that the strongly pronounced one-way transmission and reflection effects, including unidirectional transmission, can be obtained for some shapes of isofrequency contours (IFCs). These effects are associated with the different numbers of transmission channels being open when the grating is illuminated from the side of the corrugated interface and when it is illuminated from the opposite side or with the modifying effect of the back-side corrugated interface. Most part of the anomalous transmission and reflection effects can be explained, predicted, and classified using IFCs and wave-vector diagrams, despite of some skepticism concerning the possibility of using dispersion results for PC gratings.<sup>19</sup> To do this, some additional rules concerning the construction lines should be applied.

Two main classes of the one-way effects will be distinguished, depending on whether the effect of corrugations located on the front side (side of incidence) appears in the transmitted far field or not. Correspondingly, they are referred to as *translation* and *isolation* regimes. Alternatively, the effects predictable using IFCs can be classified directly in the terms of IFC features. Examples will also be considered for the situations, when the isolation and translation regimes appear, but cannot be predicted using IFCs. It will be demonstrated that more than a half of the incident-wave energy can be transmitted in one direction only, for both IFCs located near  $M$  point and  $X$  point of the first Brillouin zone (FBZ). Contrary to the unidirectionality, which can be obtained using anisotropic materials, no change of linear polarization appears in the suggested approach. All the waves involved to the diffraction are linearly polarized. Consideration

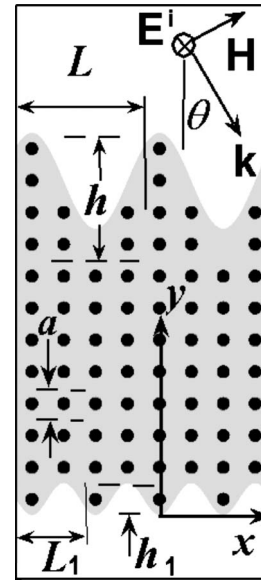


FIG. 1. PC with periodically corrugated upper and lower interfaces.

is restricted to square-lattice PCs made of isotropic dielectrics and  $s$  polarization of the incident waves. The presented near- and far-field results are obtained using the fast coupled-integral-equations technique.<sup>35</sup> To obtain IFCs and wave-vector diagrams, CST MICROWAVE STUDIO software<sup>36</sup> and a self-made postprocessing program have been used.

## II. THEORETICAL BACKGROUND

Consider diffraction of the  $s$ -polarized plane wave, which is incident from the upper half space ( $y > D$ ,  $D = Pa$ ,  $a$  is lattice constant, and  $P$  is number of the rod layers at  $x=0$ ), on the PC grating as shown in Fig. 1. PC is composed of circular dielectric rods, which are arranged to square lattice.

The fundamental difference between the finite-thickness gratings made of conventional isotropic dielectrics (index of refraction  $N > 1$ ), on the one hand, and those made of noble metals, ultralow-index and (near-)zero-index metamaterials, and PCs operating in the ultralow-effective-index regime ( $0 < \text{Re } N < 1$ ),<sup>30,37,38</sup> on the other hand, is the following. In the former case, isotropic (circular) IFCs in the dielectric medium show a larger radius than that in air so that all the propagating orders and some evanescent orders in air are coupled to the waves propagating in the dielectric. As a result, the transmitted field can be affected by the topological features of the front-side interface, showing the presence of those orders in far field, which are dictated by its period of corrugations. In other words, the periodic features are *translated* to the lower (transmission) half space.

In the contrast, the IFCs in the latter case are narrower than in air. As a result, only a single order propagating in the half space of incidence can be coupled to a propagating FB wave. If this is zero order, the transmitted far field does not contain the orders, which could appear due to the front-side corrugations, so that the upper and lower half spaces are *isolated* from each other. In fact, the appearance of the iso-

lation regime is not restricted to the structures with the periodically corrugated interfaces. It has recently been shown that the slabs and shells of rather various shapes, which are made of  $\epsilon$ -near-zero materials, can efficiently isolate the regions of space they delimit.<sup>39</sup>

In turn, PCs can show not only a circular shape of IFCs and hence a richer variety of the order-selectivity diffraction effects is achievable in PC gratings than in the gratings made of homogeneous materials. For example, the number of reflected beams and the number of the refracted beams inside a PC can show various combinations even in case without corrugations.<sup>40,41</sup>

The electric field in the upper and lower ( $y < 0$ ) half spaces is presented as follows:

$$E(x, y) = E^i(x, y) + \sum_{n=-\infty}^{\infty} \rho_n \exp(i\alpha_n x + i\eta_n y), \quad (1)$$

and

$$E(x, y) = \sum_{n=-\infty}^{\infty} \tau_n \exp(i\alpha_n x - i\eta_n y). \quad (2)$$

Here,  $\eta_n = \sqrt{k^2 - \alpha_n^2}$ ,  $\text{Im } \eta_n \geq 0$ ,  $\alpha_n = \alpha_0 + 2\pi n/L$ ,  $\alpha_0 = k \sin \theta$ ,  $k$  is free-space wave number,  $\theta$  is the angle of incidence,  $L$  is grating period,  $\rho_n$  and  $\tau_n$  are amplitudes of the  $n$ th-order beams in reflection and transmission, respectively. In Eqs. (1) and (2),  $\eta_n$ ,  $\alpha_n$ , and  $2\pi n/L$  are the perpendicular and parallel components of wave vector and a reciprocal-lattice vector of a one-dimensional periodic structure with period  $L$ , respectively. Details of the field representation at  $0 < y < D$  can be found in Ref. 35. The incident wave is given by  $E^i(x, y) = E_0 \exp(i\alpha_0 x - i\eta_0 y)$ , where  $\eta_0 = k \cos \theta$  and  $E_0$  means amplitude.

To characterize transmission and reflection in a multibeam regime, we use values of diffraction efficiency<sup>42</sup>

$$r_n = \rho_n \rho_n^* \text{Re } \eta_n / \mathcal{W}, \quad (3)$$

and

$$t_n = \tau_n \tau_n^* \text{Re } \eta_n / \mathcal{W}, \quad (4)$$

where  $\mathcal{W}$  is the energy of the incident wave and asterisk means complex conjugate. In a lossless case,  $\mathcal{R} + \mathcal{T} = \mathcal{W}$ , where the reflectance  $\mathcal{R} = \sum_{n=-\infty}^{\infty} r_n$  and the transmittance  $\mathcal{T} = \sum_{n=-\infty}^{\infty} t_n$ . According to the FB theorem, a wave propagating inside an infinite PC has the form of a FB wave, i.e.,

$$E_{z,h} = \exp(i\mathbf{k}_h^{\text{PC}} \mathbf{r}) \sum_G A_G(\mathbf{k}_h^{\text{PC}}) \exp(i\mathbf{k}_h^{\text{PC}} \mathbf{G}), \quad (5)$$

where  $\mathbf{k}_h^{\text{PC}}$  is wave vector of the  $h$ th FB wave (PC pass band) and  $\mathbf{G}$  is a reciprocal-lattice vector.

In the considered PC gratings, large- and small-period corrugations may appear on the both sides. The periods are related to each other as follows:

$$L = mL_1, \quad (6)$$

where  $m = 2, 3, \dots$  so that any structure remains periodic in  $x$  direction. If  $L_1 = a$  in Eq. (6), a virtual interface is considered to be noncorrugated. For the sake of convenience, we assume

TABLE I. Nomenclature of PC gratings.

	Upper	Lower	Upper	Lower
CU	+	−	$L$	$a$
CL	−	+	$a$	$L$
CUL	+	+	$L$	$L_1$
CLU	+	+	$L_1$	$L$

that a PC grating is obtained by removing certain rods from a  $P$ -layer PC without corrugations, i.e., with  $L = L_1 = a$ . The depths of corrugation for the interfaces with periods  $L$  and  $L_1$  are given by  $h = pa$  and  $h_1 = p_1 a$ , where  $p, p_1 = 1, 2, 3, \dots$  and  $p + p_1 \leq P$ . If the host medium has permittivity  $\epsilon_h \neq 1$ , the rods are inserted, in fact, into a grating made of a homogeneous material so that the depths of the grating corrugations can differ from  $h$  and  $h_1$ . If  $\epsilon_h = 1$ , an effective interface cannot be introduced in an unambiguous way.

The structure nomenclature is given in Table I. It depends on whether the corrugations appear on the front (upper) side, back (lower) side, or the both sides of the PC grating. Here, CU and CL correspond to the PC gratings with corrugated upper and lower interface, respectively. CUL and CLU correspond to the gratings with corrugated upper and lower interfaces, and with corrugated lower and upper interfaces, respectively, where the first mentioned interface has larger period. Signs + and − in the second and third columns indicate the presence or absence of corrugations at the corresponding interface, respectively. In the fourth and fifth columns, the longitudinal periods are given. In line with the used nomenclature, the structure in Fig. 1 is a CUL structure. It is assumed that

$$L_1 = la, \quad (7)$$

where  $l = 2, 3, \dots$  so that  $L = mla$ .

According to the general theory of diffraction gratings,<sup>42</sup> the  $n$ th-order beams may propagate if

$$k > |\alpha_0 + 2\pi n/L|. \quad (8)$$

The  $n$ th-order Rayleigh wavelength, which splits the propagating-wave and evanescent-wave regimes, corresponds to

$$k_n(L, \theta) = 2\pi|n|/L(1 \pm |\sin \theta|), \quad (9)$$

where the signs + and − stand for the cases with  $\text{sgn } n \neq \text{sgn } \theta$  and  $\text{sgn } n = \text{sgn } \theta$ , respectively. The angles of diffraction of the reflected beams are given by

$$\sin \phi_n = \sin \theta + 2\pi n/kL. \quad (10)$$

The angles  $\phi_n$  and  $\theta$  are measured from the positive-valued part of  $y$  axis in Fig. 1 in the clockwise and counterclockwise directions, respectively. The angles of diffraction of the  $n$ th-order transmitted beams  $\hat{\phi}_n$  are measured from the negative-valued part of  $y$  axis in the counterclockwise direction, i.e.,  $\hat{\phi}_n = \phi_n$ .

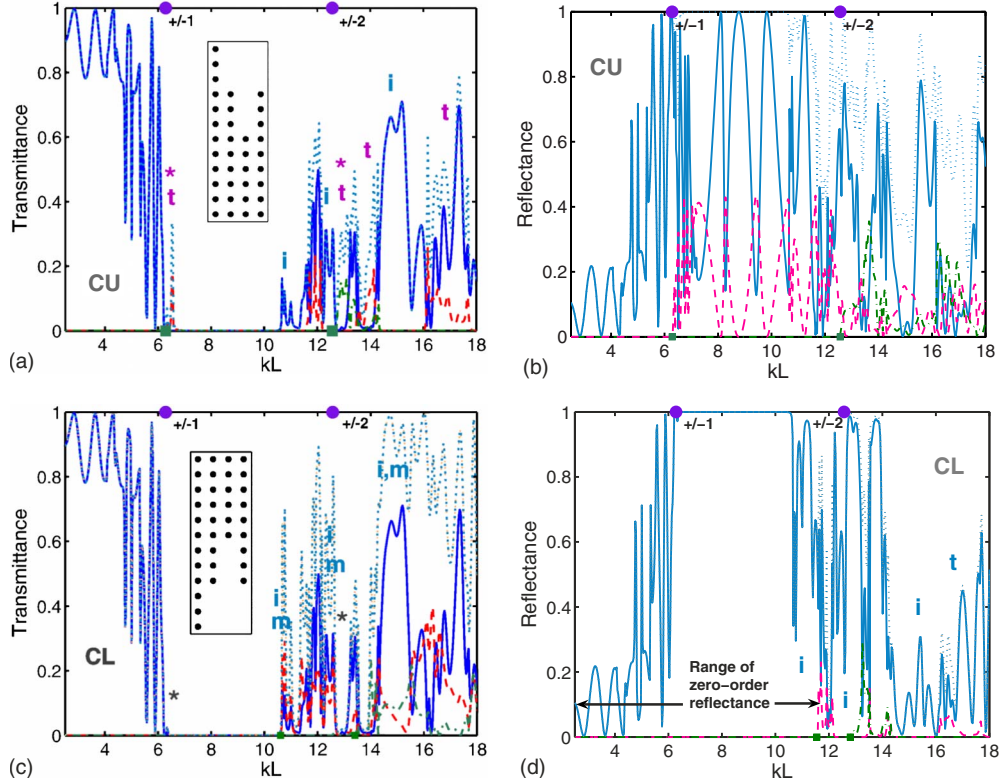


FIG. 2. (Color online) Transmittance and reflectance for PC grating with  $P=12$ ,  $d/a=0.4$ ,  $\epsilon_r=11.4$ , and  $\theta=0$ ;  $h/D=0.5$  and  $h_1/D=0$ ,  $L=4a$  and  $L_1=a$ ; solid, dashed, and dash-dotted lines correspond to  $n=0$ ,  $n \pm 1$ , and  $n \pm 2$ , respectively; dotted lines— $\mathcal{T}$  in plots (a) and (c) and  $\mathcal{R}$  in plots (b) and (d); insets show composition of the rods within a grating period; circles— $k_{\pm 1}$  and  $k_{\pm 2}$ ; squares— $\kappa_{\pm 1}$  and  $\kappa_{\pm 2}$ .

Corrugations result in a shift of the range of multibeam regime toward smaller frequencies. Indeed, in case of a non-corrugated PC, we have

$$k > |\alpha_0 + 2\pi n/a| \quad (11)$$

and

$$k_n(a, \theta) = 2\pi|n|/a(1 \pm |\sin \theta|), \quad (12)$$

instead of Eqs. (8) and (9). For example,  $k_n(L, \theta)/k_n(a, \theta) = a/L$  at  $\theta=0$ .

Using corrugations, the Rayleigh wavelength at a fixed  $n$  can be shifted down to the first pass band of PC even at  $\theta=0$ . However, contribution of some orders to  $\mathcal{T}$ , which are propagating according to Eq. (8), is vanishing within wide ranges of  $kL$  variation, that are referred to as nonordinary ORs and connected with the one-way transmission.<sup>19</sup> The ORs can be located in such a manner that for some orders  $\kappa_n > k_n$ , where  $\kappa_n$  is wave number, starting from which the  $n$ th order actually contributes to  $\mathcal{T}$  or  $\mathcal{R}$ . Throughout the paper, a value of  $k$  corresponding to the middle of an ordinary or nonordinary OR is denoted by  $K$ .

Two following reciprocity conditions are important for our study, which are valid for rather arbitrary finite-thickness gratings. They are

$$t_0^{\rightarrow} = t_0^{\leftarrow} \quad (13)$$

for all  $k$  and

$$r_0^{\rightarrow} = r_0^{\leftarrow} \quad (14)$$

for  $k < k_{-1}$ . The two directions of the arrows correspond to the two opposite orientations of the incident wave. In terms of the nomenclature in Table I, they correspond to a pair of structures CU and CL, or CUL and CLU.

Such reciprocity does not occur for higher-order transmittance and reflectance so that  $t_n^{\rightarrow} \neq t_n^{\leftarrow}$  and  $r_n^{\rightarrow} \neq r_n^{\leftarrow}$  at  $|n| > 0$ . These conditions give a recipe for obtaining *unidirectionality*, i.e.,  $\mathcal{T}^{\leftarrow} = 0$  while  $\mathcal{T}^{\rightarrow} \neq 0$ . To realize this regime, it should be necessary (but not sufficient) that zero order does not contribute to  $\mathcal{T}$ , being uncoupled to a FB wave of PC. This feature cannot be realized using a homogeneous medium with  $N > 1$  but is well consistent with some IFC shapes, which can be obtained using PCs. Behavior of  $t_{\pm 1}$  at  $kL = 6.5$  in Fig. 4 from Ref. 19 (there  $\mathcal{T}^{\text{CU}} \approx 0.35$  and  $\mathcal{T}^{\text{CL}} = 0$ ) is in agreement with this expectation.

### III. NUMERICAL RESULTS AND DISCUSSION

#### A. PC gratings with one corrugated interface

First, we will demonstrate the anomalous one-way diffraction effects, which are typical for PC gratings with one-side corrugations. As an example, we consider diffraction on the grating, which differs from one of those in Ref. 19 in value of  $P$  while  $h/D$  and lattice parameters are kept the same. Figure 2 shows  $t_n$  and  $r_n$  vs  $kL$  in CU and CL cases at  $\theta=0$ . The five first FB waves (PC bands) contribute to the

transmission within the considered  $kL$  range. The main attention is paid for the nonordinary ORs, in which wideband suppression occurs for one or several orders that may propagate in line with the conventional grating theory, and which could be connected with the one-way diffraction effects. Such ranges appear in the vicinity of  $KL=6.5$  ( $t_0=0$ ),  $KL=11$ ,  $12.5$ , and  $15$  ( $\mathcal{T}\approx t_0$ ,  $K>k_{\pm 1}$ ), and  $KL=17$  ( $\mathcal{T}\approx t_0+t_1+t_{-1}$ ,  $K>k_{\pm 2}$ ). They do not vary within a wide range of variation in  $P$  and, hence, are related to certain features of IFCs. Origin of the narrow ranges with  $\mathcal{T}\approx t_{-2}+t_2$  in the vicinity of  $kL=12.8$  and with  $\mathcal{T}\approx t_{-1}+t_{+1}$  in the vicinity of  $kL=13.8$  will be discussed later.

The nonordinary ORs arising at  $kL=11$ ,  $12.5$ , and  $15$  are associated with the isolation regime since the spatial structure of far field at  $y<0$  is not affected by the periodic features of the upper-side interface (they are marked by **i**). The ranges arising at  $KL=6.5$  and  $KL=17$  can be assigned to the translation regime since the transmitted far field contains the orders arising due to the upper-side corrugations (they are marked by **t**). Note that the ranges of one-way transmission are wider than those obtained earlier for the branched-slit gratings in Ref. 22.

It is demonstrated in Fig. 2(b) that all the orders satisfying Eq. (8) contribute to  $\mathcal{R}$ , regardless of that whether the considered  $kL$  range coincides with a nonordinary OR in transmission or not. This feature also occurs in the CL-case transmission. The dependence of  $t_n$  on  $kL$  is shown in this case in Fig. 2(c). One can see that most of the nonordinary ORs disappear, when the spatial structure of the transmitted far field can be modified due to the effect of the corrugated back-side interface so that the orders suppressed by PC contribute to  $\mathcal{T}^{\text{CL}}$  (the corresponding ranges are marked by **m**). At the same time,  $\mathcal{R}\approx r_0$  in these ranges, see Fig. 2(d).

Two cases can be distinguished in the translation regime. One of them can be illustrated by the nonordinary OR at  $KL=17$ , where  $\mathcal{T}^{\text{CU}}\approx\sum_{n=-1}^1 t_n$  but  $\mathcal{T}^{\text{CL}}\approx\sum_{n=-2}^2 t_n$ . Therefore, the effect of corrugations occurs for the both orientations of the corrugated interface with respect to the incident wave. We refer to this regime as *bidirectional translation*. In the contrast,  $\mathcal{T}^{\text{CU}}=t_{-1}+t_{+1}$  and  $\mathcal{T}^{\text{CL}}\approx 0$  at  $KL=6.5$ . Similar situation takes place in the vicinity of  $kL=12.8$  and  $kL=13.8$ . Such regimes can be referred to as *unidirectional translation* (two of the corresponding  $kL$  ranges are marked by \*). As was expected, the unidirectionality appears while  $t_0^{\text{CU}}=t_0^{\text{CL}}=0$ . Hence, this regime can be considered in terms of *light deflection*.<sup>43</sup> Indeed, transmission at  $\theta=0$  is exclusively realized due to the deflected beams,  $\phi_{\pm 1}\neq 0$ .

Some kind of *duality* can be seen in Fig. 2, which manifests itself in that the location of nonordinary ORs in transmission in CU case coincides with those in reflection in CL case, provided that they are connected with the isolation regime. Simultaneous existence of translation and isolation within different  $kL$  ranges results in the anomalous location of the values of  $\kappa_n$ , e.g.,

$$\kappa_{\pm 1}^{\text{CU}}(T) < \kappa_{\pm 1}^{\text{CL}}(T) < \kappa_{\pm 1}^{\text{CL}}(R),$$

where  $T$  and  $R$  correspond to transmission and reflection, respectively. In turn, in CL case,

$$k_{\pm 1} < \kappa_{\pm 1}(T) < \kappa_{\pm 1}(R). \quad (15)$$

At the same time, in CU case,

$$k_{\pm 1} \approx \kappa_{\pm 1}(T) \approx \kappa_{\pm 1}(R), \quad (16)$$

so that the appearance of nonordinary ORs does not lead to the shift of the values of  $\kappa_{\pm 1}$  with respect to  $k_{\pm 1}$ .

### B. Conditions of one-way diffraction regimes

Consider now the possibility of prediction of the anomalous diffraction effects, which appear at  $\theta=0$  due to corrugations, by using dispersion results. To do this, the features of IFCs and wave-vector diagrams in  $\mathbf{k}$  space will be compared with the transmission results in several peculiar cases in Fig. 2. The commonly used rules of plotting IFCs can be found in the PC relevant literature, e.g., see Refs. 41, 44, and 45. In particular, conservation of the parallel component of wave vector  $k_x$  and restriction of the consideration to the crossing points of IFCs with the construction lines, which satisfy the causality principle (the energy velocity  $\mathbf{v}_e$  must be pointed away from the source), will be used. For a noncorrugated PC, the IFC at a fixed  $\omega$ , fixed band slope (sign of  $\nabla_{\mathbf{k}}\omega\cdot\mathbf{k}^{\text{PC}}$ , where  $\mathbf{k}^{\text{PC}}$  is wave vector of a FB wave), and gradient of IFCs at fixed  $k_x^{\text{PC}}$  are considered to be sufficient for determining all refracted beams.<sup>41</sup> For PC gratings, the set of construction lines should involve those for the diffraction orders, which might be propagating due to corrugations. It will be shown that in order to properly account for the effect of the interfaces, construction lines should be plotted by taking into account the IFC topology.

An example is shown in Fig. 3, where three cases with various topologies are presented, which all correspond to the isolation regime. The wave vectors for the  $n$ th-order diffracted beams  $\mathbf{k}_n$  and gradients of the group velocity  $\mathbf{v}_g=\mathbf{v}_e$  (see Ref. 46) inside a PC are shown. Values of  $n$  at a plot top ( $-2, -1, 0, +1, +2$ ) correspond to the orders, which should be propagating according to Eq. (8). The large blue numbers (2,3,4) mean a number of FB wave (PC pass band). For the groups of the embedded contours, the most outer contour at  $X$  or  $\Gamma$  point in plots (a) and (c) and the most inner contour at  $\Gamma$  point in plot (b) correspond to largest  $kL$ .

For all three cases in Fig. 3, only zero order is coupled to a FB wave at  $k=\hat{k}$ . Transmission is realized due to the sole transmission channel at  $n=0$ , whatever CU case or CL is considered, like it would occur in the corresponding PC without corrugations. At the same time, Fig. 2(c) shows that the orders with  $n=\pm 1, \pm 2$  contribute to  $\mathcal{T}$  in CL case. This occurs owing to diffraction on the corrugated back-side interface. In other words, not all orders in the transmission half space should be themselves coupled to a FB wave. All ranges of isolation in Fig. 2 are in good agreement with the wave-vector diagrams. This remains true for the results presented in Ref. 19.

Using the IFC results, the following *conditions of the existence of isolation regime* can be formulated at  $\theta=0$  and  $ka\leq\pi$ : (i) IFCs must contain those centered around  $\Gamma$  or  $X$  point; (ii)  $k>|\alpha_0+2\pi n/L|$  for at least one pair of the orders with  $\pm n, |n|>0$ ; (iii)  $k_{\min,x}^{\text{PC},2}>|k\sin\phi_{\pm n}|>k_{\max,x}^{\text{PC},1}$  for all or-

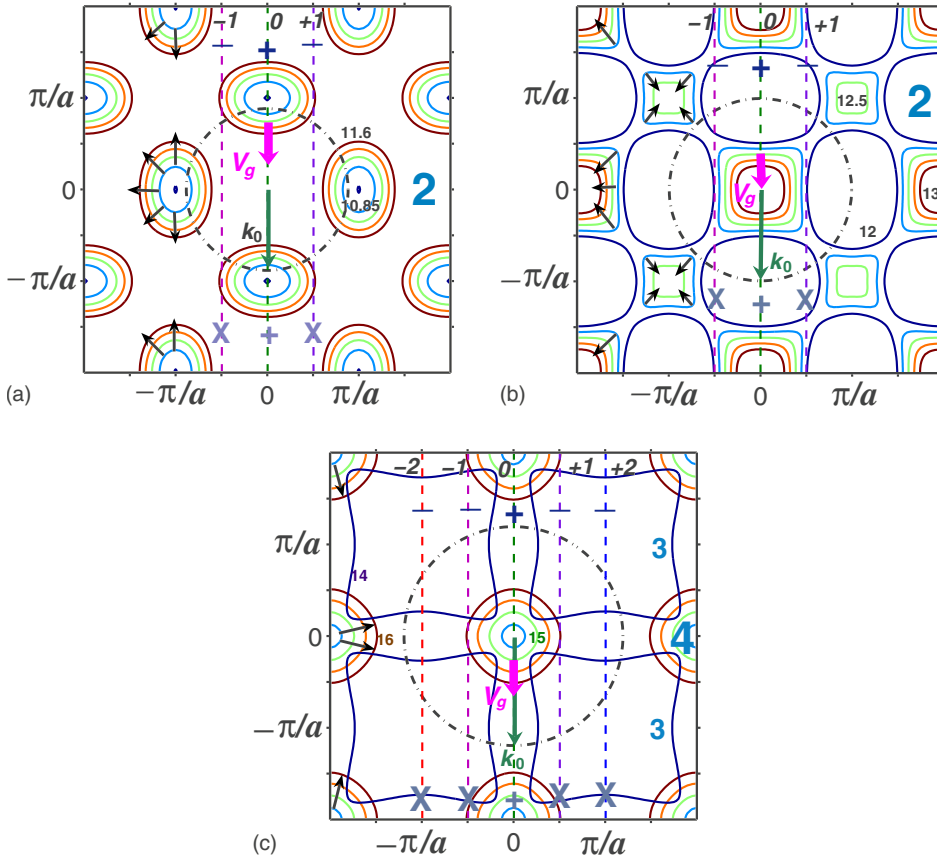


FIG. 3. (Color online) IFCs in isolation regime (solid lines) on plane  $(k_x, k_y)$  at  $d/a=0.4$ ,  $\varepsilon_r=11.4$ , and  $ml=4$ : case (a)— $kL=10.6, 10.85, 11.1, 11.35$ , and  $11.6$ ; case (b)— $kL=12, 12.25, 12.5, 12.75$ , and  $13$ ; case (c)— $kL=14, 14.5, 15, 15.5$ , and  $16$ ; wave-vector diagrams are shown at (a)  $kL=\hat{k}L=11.1$ , (b)  $12.5$ , and (c)  $15$ ; dash-dotted circles—IFCs in air; vertical dashed lines—construction lines at  $\theta=0$ ; intermediate-width and thick arrows—directions of  $\mathbf{k}_n$  and  $\mathbf{v}_g$  in CU case at  $n=0$  and  $k=\hat{k}$ , respectively; thin arrows—gradients of  $\mathbf{v}_g$ ; signs + and - at the top (CU case) and the bottom (CL case) mean coupling and noncoupling to a FB wave, respectively; sign  $\times$  at the bottom (CL case) indicates the orders, which may not appear due to the effect of the noncorrugated interface.

ders satisfying condition (ii), where  $k_{\max,x}^{\text{PC},1}$  and  $k_{\min,x}^{\text{PC},2}$  mean maximal  $k_x^{\text{PC}}$  of the contour around  $\Gamma$  point or  $X$  point at  $k_x=0$ , and minimal  $k_x^{\text{PC}}$  of the contour around  $M$  point or  $X$  point at  $k_x=\pi/a$ , respectively; (iv) the back-side interface must be noncorrugated, i.e.,  $L_1=a$ .

For the definiteness sake, we assume that  $k_x^{\text{PC}} > 0$  in these and other similar conditions presented in this paper. The conditions (i)–(iv) can be used at least if one FB wave and no more than two groups of IFCs are existing within the considered  $kL$  range, e.g., see Figs. 3(a) and 3(b). They can be generalized for different lattice types and IFC topologies. If there is only one group of IFCs, as in Fig. 3(c) at  $k=\hat{k}$ , the conditions (i)–(iv) can also be used while the incident-wave vector is extended beyond the FBZ, e.g., at

$$k < 2\pi/a - k_{\max,x}^{\text{PC},1}, \quad (17)$$

provided that  $k_{\min,x}^{\text{PC},2}=k$  is formally taken in the condition (iii).

The closer shape of the IFCs being centered around  $\Gamma$  point to a circle, the more robust should be the existence of the isolation regime to a variation in the angle  $\delta$  between  $\Gamma$ - $X$  direction and  $x$  axis (up to now it was  $\delta=0$ ). For example, one could vary  $\delta$  from 0 to  $\pi/4$  at least at  $14 < kL < 15$  in Fig. 3(c). In the contrast, using  $\delta=\pi/4$  in Fig. 3(a) results in the disappearance of the isolation regime. In particular,  $\mathcal{T}^{\text{CU}} \approx 0$  at  $kL=10.6$  and  $kL=10.85$  while  $\mathcal{T}^{\text{CU}} > 0$  and  $t_0^{\text{CU}} = 0$  at  $kL=11.1, 11.35$ , and  $11.6$ .

Figure 4 shows the near-field pattern, which is typical for the isolation regime. Topology within the regular region of the PC ( $0 < y < Pa/2$  in CU case and  $Pa/2 < y < Pa$  in CL

case) and that within the corrugated region of the PC ( $Pa/2 < y < Pa$  in CU case and  $0 < y < Pa/2$  in CL case) are substantially different. It is seen that the corrugated interface is responsible for the field features related to the contribution of higher orders to  $\mathcal{R}$  in CU case and to  $\mathcal{T}$  in CL case while the same FB wave determines the field pattern within the regular region, preventing appearance of higher orders in the half space bounded by a noncorrugated interface. This remains true for all the cases in Fig. 2 where the isolation regime does appear.

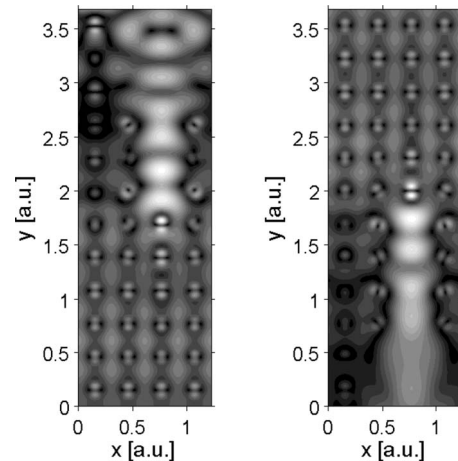


FIG. 4. Electric field at  $0 < x < L$ ,  $0 < y < Pa$ , and  $kL=15$  in CU case (left) and CL case (right) from Fig. 2;  $\mathcal{T}^{\text{CU}}=t_0$  and  $\mathcal{T}^{\text{CL}}=t_0 + t_{-1} + t_{+1} + t_{-2} + t_{+2}$ .

There are various physical situations, which are associated with the isolation regime and the corresponding one-way transmission. For example, it can appear at the both signs of  $\mathbf{S} \cdot \mathbf{k}^{\text{PC}}$ , where  $\mathbf{S}$  is Poynting vector. In Fig. 3(c), we have  $\mathbf{S} \cdot \mathbf{k}^{\text{PC}} > 0$  and  $N_{\text{eff}} \approx 0.22$  at  $kL = \hat{k}L = 15$ . In Figs. 3(a) and 3(b), the isolation is achieved at  $\mathbf{S} \cdot \mathbf{k}^{\text{PC}} < 0$  while phase and group velocities are antiparallel. Therefore, the isolation effect is necessarily connected with neither an ultralow-effective-index behavior nor the handedness. However, IFCs for the PC must be narrower than those for air, providing that higher orders are not coupled. Furthermore, the isolation occurs while  $N$  tends to zero, i.e., IFCs are vanishing (compare to Ref. 30).

Examples of IFCs corresponding to the translation regime are presented in Fig. 5. From the comparison of Fig. 5(a) with Fig. 2, the signature of the *unidirectional translation* arising at  $kL = 6.5$  is clearly seen. The construction lines are plotted by taking into account the period of an interface of incidence. In the CU case, only the orders with  $n = \pm 1$ , which appear due to diffraction on the front-side corrugated interface, are coupled to a FB wave. In the CL case, the sole existing order is not coupled to a FB wave while the effect of the opposite-side (corrugated) interface is absent so that  $\mathcal{T}^{\text{CL}} = 0$ .

Hence, the following *conditions of unidirectional translation* are valid at  $ka \leq \pi$ ,  $\theta = 0$ , and  $\delta = 0$ : (i) IFCs are centered around  $M$  point; (ii)  $k > |\alpha_0 + 2\pi n/L|$  at least for one pair of the orders  $\pm n$ ,  $|n| > 0$ ; (iii)  $k_{\text{max},x}^{\text{PC}} > |k \sin \phi_{\pm n}| > k_{\text{min},x}^{\text{PC}}$  for at least one pair of the orders  $\pm n$ ,  $|n| > 0$ , where  $k_{\text{min},x}^{\text{PC}}$  and  $k_{\text{max},x}^{\text{PC}}$  mean minimal and maximal  $k_x^{\text{PC}}$  for IFCs at given  $ka$ ; (iv) no FB wave may be coupled to zero order, i.e.,  $k_{\text{min},x}^{\text{PC}} > 0$ ; (v) the upper (front-side) interface must be corrugated.

In Fig. 5(a),  $\mathbf{S} \cdot \mathbf{k}^{\text{PC}} > 0$ , two transmission channels are open, and, hence, two beams contribute to  $\mathcal{T}^{\text{CU}}$ . The both beams are deflected, i.e.,  $\phi_n \neq \theta$ , that is distinguished from the conventional dielectric gratings. Now, at the front-side interface every beam mimicks refraction at small nonzero  $\theta$ , which would appear at a virtual flat interface between air and a low-index medium. The birefringence appears due to the sole FB wave while the two deflected beams show here  $|\phi_{\pm 1}| = 74.2^\circ$  at  $kL = 6.53$ . The features of refraction on the back-side (noncorrugated) interface are typical for a flat interface between a low-index medium and air.

It is worth noting that the IFCs in Fig. 5(a) have similar topology as those for TE modes in PCs from Ref. 45. Ac-

cordingly, the IFCs are similar to the IFCs for a homogeneous medium, for which hyperbolic-type dispersion occurs owing to anisotropy of the used material.<sup>47</sup> This analogy has been demonstrated in Ref. 45 by comparing with TE modes in a nonmagnetic material. In this case,

$$\tilde{\epsilon} = \begin{pmatrix} \epsilon_1 & 0 \\ 0 & \epsilon_2 \end{pmatrix} \quad (18)$$

with  $\epsilon_1 > 0$  and  $\epsilon_2 < 0$ , leading to a dispersion relation  $k_2^2 / \epsilon_1 - k_1^2 / |\epsilon_2| = \omega^2 / c^2$ . Similar analogy occurs for modes of the other polarization.

From the presented results, one can see that anisotropic-like IFCs of PC is a signature of the unidirectional transmission. However, the former is not sufficient for the appearance of the latter. One-side corrugations are needed. On the other hand, it can be shown that the IFCs centered around  $M$  point are not necessary for achieving unidirectionality. For example, the required hyperbolic-type IFCs can be obtained if the IFCs are centered around  $X$  point at  $\delta = \pi/4$ , e.g., see Fig. 3(a).

Figure 5(b) illustrates another manifestation of the translation regime, which occurs at  $kL = \hat{k}L = 17$ , where  $N_{\text{eff}} \approx 0.55$ . Here, the transmitted far field in CU case is affected by the upper-side corrugations due to the orders with  $n = \pm 1$ , which are coupled to a FB wave, as well as zero order. There are three transmission channels, which appear owing to the same FB wave showing  $\mathbf{S} \cdot \mathbf{k}^{\text{PC}} > 0$ . One of them is connected with the transmitted beam, for which  $\phi_n = 0$ , that is typical for the conventional dielectric gratings. In fact, the channels with  $n = \pm 1$  can be considered as those mimicking a positively and negatively refracted beam at a virtual flat upper-side interface at  $\theta \neq 0$ .

To understand how the construction lines should be used in this case, we consider near-field patterns corresponding to  $k = \hat{k}$  from Fig. 5(b)—see Fig. 6. The principal difference between the CU and CL cases is observed for the nonregular (corrugated) regions. On the other hand, analysis of the field topology within the regular regions shows that more than one transmission channel contributes to the transmission in both CU and CL cases. In turn,  $r_{\pm 1} \neq 0$  in the vicinity of  $k = \hat{k}$ . This conclusion is confirmed by the field pattern for the corresponding noncorrugated PC (not shown). Therefore, the periodic features of the both front- and back-side interfaces of PC grating have to be taken into account by the construc-

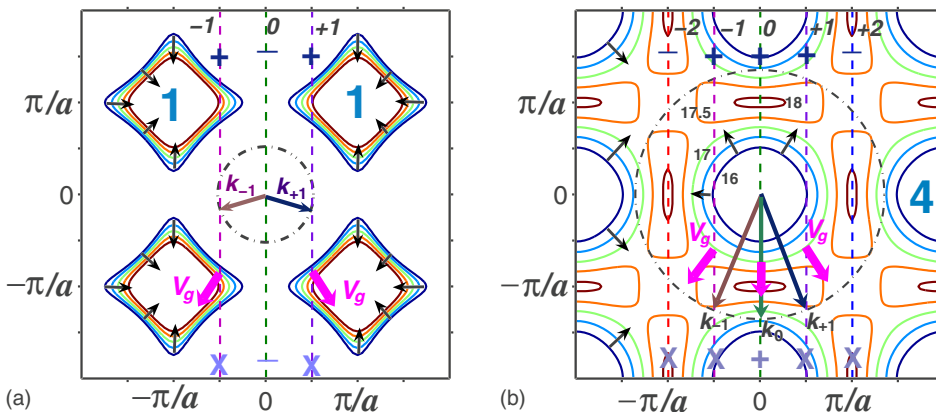


FIG. 5. (Color online) IFCs in translation regime at  $d/a = 0.4$ ,  $\epsilon_r = 11.4$ , and  $ml = 4$ : in case (a) at  $kL = 6.35, 6.44, 6.53, 6.62$ , and  $6.71$ ; in case (b) at  $kL = 16, 16.5, 17, 17.5$ , and  $18$ ; directions of  $\mathbf{k}_n$  and  $\mathbf{v}_g$  in CU case and corresponding IFCs in air are shown at (a)  $kL = \hat{k}L = 6.53$  and (b)  $17$ ; notations are the same as in Fig. 3.

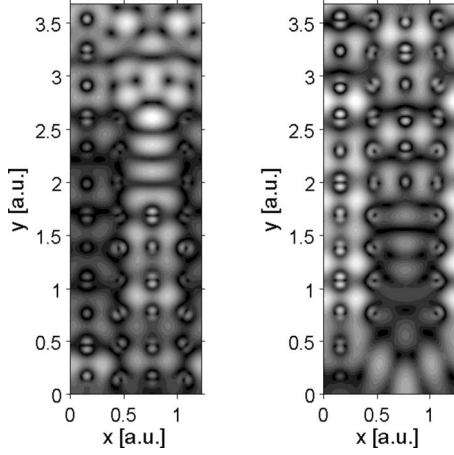


FIG. 6. Electric field at  $0 < x < L$ ,  $0 < y < Pa$ , and  $kL=17$  in CU case (left) and CL case (right) from Fig. 2.

tion lines. The regime occurring at  $kL=17$  can be classified as *bidirectional translation*. In fact, this situation is not distinguished from that occurring for the conventional dielectric gratings with one-side corrugations, where higher orders arising due to the effect of the back-side corrugated interface are present in the reflected far field, i.e., over the flat front-side interface.

Based on the obtained results, the following *rules* can be formulated in the two typical cases. If IFCs correspond to an effective-index behavior, at least with rather a high index, construction lines should account for the transmission channels, which can appear due to corrugations at the both front- and back-side interfaces. If dispersion is anisotropiclike, construction lines should only account for the transmission channels connected with the shape of the front-side interface.

Although most of the above-discussed transmission effects can be predicted using wave-vector diagrams with the proper construction lines, there are one-way effects, which cannot be predicted using this approach. For example, this occurs in the vicinity of  $kL=12.8$  and  $kL=13.8$ , i.e., in the cases which can also be assigned to the unidirectional translation (see Sec. III A).

The IFCs in the vicinity of  $kL=12.8$  are presented in Fig. 7. At  $k=\hat{k}$ , the orders with  $n=0$  and  $n=\pm 2$  are coupled to the second and third FB waves, respectively, for which  $\mathbf{S} \cdot \mathbf{k}^{\text{PC}} < 0$ . As a result, three transmission channels should be open in CU case. Collimation is expected to appear since direction of  $\mathbf{v}_g$  is the same for all three channels. However, one can see in Fig. 2(a) that  $\mathcal{T}^{\text{CU}} \approx t_{-2} + t_{+2}$  while  $t_0 \approx 0$  so that one of the formally open channels does not contribute to  $\mathcal{T}$ . Furthermore,  $\mathcal{T}^{\text{CL}} \approx 0$  according to Eq. (13). Hence, sometimes the unidirectionality can appear, even if this is in contradiction with the predictions based on a wave-vector diagram. At  $kL=13.8$ , the orders with  $n=\pm 2$  are coupled to the third FB wave, as well as the orders with  $n=\pm 1$ . The latter provide the main contribution to  $\mathcal{T}^{\text{CU}}$  while  $\mathcal{T}^{\text{CU}}/\mathcal{T}^{\text{CL}} > 10$ . A possible cause of this effect is that the actually contributing orders might have more preferable transmission conditions, which could be formalized, for example, in terms of the generalized effective impedance matching.

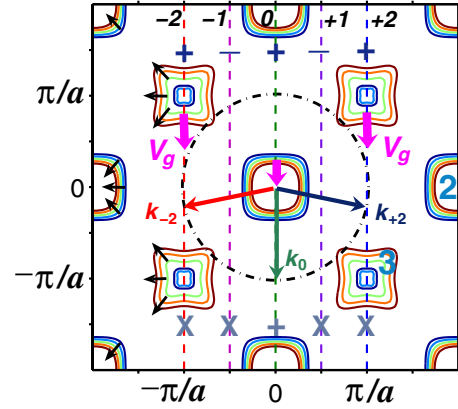


FIG. 7. (Color online) IFCs at  $d/a=0.4$ ,  $\epsilon_r=11.4$ , and  $ml=4$  at  $kL=12.6, 12.7, 12.8, 12.9$ , and  $13$ ;  $\mathbf{k}_n$  and  $\mathbf{v}_g$  in CU case, and IFC in air are shown at  $kL=\hat{k}L=12.8$ ; notations are the same as in Fig. 3; the most inner contour at  $M$  point belongs to the second FB wave.

### C. PC gratings with two-side corrugations

Consider the peculiarities of one-way diffraction in PC gratings with two-side corrugations. Let modify the CU structure in Figs. 2(a) and 2(b) in such a way that the additional corrugations appear now at the back-side interface showing the period  $L_1=2a$  and depth  $h_1=2a$  while the front-side corrugations are less deep, see the inset in Fig. 8(a). In this case, the values of  $k_{\pm 2}$  are the same as the values of  $k_{\pm 1}$  for a structure with  $L=2a$ . The CL structure from Figs. 2(c) and 2(d) is properly modified, too—see the inset in Fig. 8(c).

Dependences of  $t_n$  and  $r_n$  on  $kL$  for the obtained CUL and CLU structures are shown in Figs. 8(a)–8(d). At  $k > k_{\pm 2}$ , the orders with  $n=\pm 2$  should contribute to  $\mathcal{T}$  and  $\mathcal{R}$  within the  $kL$  ranges, where they were suppressed in CU and CL cases. In particular, this takes place within the nonordinary ORs with  $\mathcal{T} \approx t_0$  from Fig. 2, which appear in the isolation regime, e.g., at  $KL=15$  in Fig. 8(a). In fact, the isolation regime remains here although this range looks like a pass band, where the orders with  $n \neq 0$  are coupled to a FB wave and contribute to  $\mathcal{T}$ , regardless of the orientation of the interfaces with respect to the incident wave. Hence an isolation-regime transmission can be masked by the diffraction on the back-side corrugated interface.

This is illustrated by the comparison of the field patterns in CUL and CLU cases, e.g., at  $kL=15$ —see Fig. 9. The used  $kL$  value corresponds to the case when  $\mathcal{T}^{\text{CUL}} = t_0 + t_{-2} + t_{+2}$  [see Fig. 8(a)] and  $\mathcal{T}^{\text{CLU}} = t_0 + t_{-1} + t_{+1} + t_{-2} + t_{+2}$ ,  $t_{+2} \ll t_{+1}$  [see Fig. 8(c)] while only zero order is coupled to a FB wave, according to Fig. 3(c). One more range where the orders with  $n \neq 0$  now significantly contribute to  $\mathcal{T}$  is that at  $KL=17$ . At  $KL=11$ , the isolation is masked in CLU case in similar manner as in CL case in Fig. 2(c).

Comparing Figs. 8(a) and 8(c) with Figs. 2(a) and 2(c), one can see that the nonordinary ORs in the vicinity of  $kL=12.8$  and  $kL=13.8$  are strongly sensitive to an interface shape. The former range is located now near  $kL=12.4$ , i.e., it is shifted toward smaller  $kL$ . Furthermore, now it is bidirectional. The latter one disappears so that  $t_n \neq 0$  at  $|n|=1, 2$  in the vicinity of  $kL=13.8$ . No new feature appears in reflection

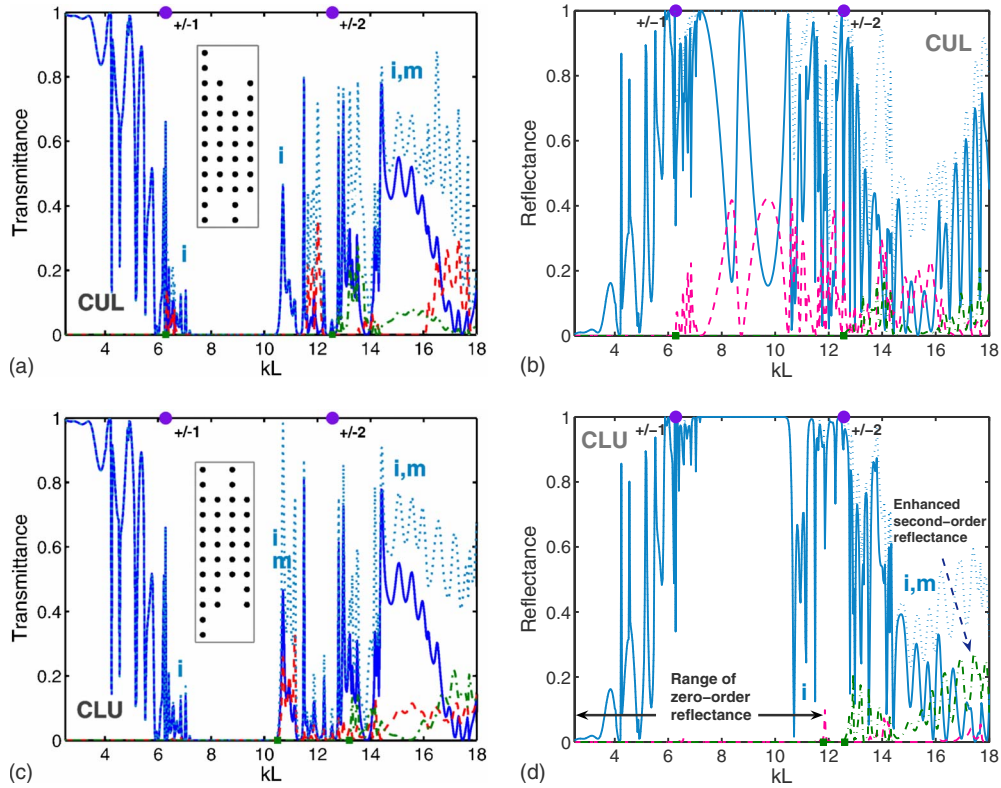


FIG. 8. (Color online) Same as Fig. 2 but for CUL and CLU cases instead of CU and CL cases, respectively;  $h/D=1/3$ ,  $h_1/D=1/6$ ,  $L=4a$ , and  $L_1=2a$ .

in CUL case as compared to CU case. Locations of  $\kappa_n$  are either slightly affected or not affected at all by adding new corrugations in both CUL and CLU cases.

The zero-order transmission takes place in CUL and CLU cases at  $2\pi < kL < 7.22$ , where  $t_0=0$  in CU and CL cases, and for the corresponding noncorrugated PC. This range can be considered as a new nonordinary OR in transmission since  $\mathcal{T}^{\text{CUL}}=t_0+t_{-1}+t_{+1}$  and  $\mathcal{T}^{\text{CLU}}=t_0$  at  $2\pi < kL < 6.74$  (one-way transmission for the orders with  $n=\pm 1$ ), and  $\mathcal{T}^{\text{CUL}}=\mathcal{T}^{\text{CLU}}\neq 0$  at  $6.74 < kL < 7.07$  and  $7.15 < kL < 7.22$  (two-way transmission). The fact that  $\mathcal{T}$  is nonzero at the  $kL$  values, at which  $\mathcal{T}$  is zero in CU case, cannot be explained using a wave-vector diagram like that in Fig. 5. Perhaps, it is related to the effect of corrugations with  $L_1 > a$  and  $h_1 \neq 0$ , which themselves represent a rectangular periodic lattice that can show pass and stop bands being different from those of the basic square-lattice PC.

**D. Improved unidirectionality**

The unidirectional transmission can be enhanced due to a proper choice of lattice parameters. In particular, larger  $\mathcal{T}^{\text{CU}}$  and a wider  $kL$  range, within which  $\mathcal{T}^{\text{CU}} > 0$  and  $\mathcal{T}^{\text{CL}} \approx 0$ , can be obtained for smaller  $\epsilon_r$  and same remaining parameters as in Fig. 2. Figure 10 shows  $t_n$  vs  $kL$  in CU and CL cases at  $\epsilon_r=5.8$ . The unidirectional translation occurs here at  $KL=8.6$  and  $KL=17$ . For example,  $\mathcal{T}^{\text{CU}}=t_{-1}+t_{+1}\approx 0.63$  at  $kL=8.6$ , and  $\mathcal{T}^{\text{CU}}\approx 0.6$  and  $0.7$  at  $KL=17$  and  $KL=17.5$ , respectively. In the latter case, all four higher propagating orders are translated so that the *multibeam unidirectionality* is

achieved. Furthermore, the ranges with  $\mathcal{T}^{\text{CU}}\approx t_{-2}+t_{-1}+t_{+1}+t_{+2}$  and  $\mathcal{T}^{\text{CU}}\approx t_{-2}+t_{+2}$  are adjacent, i.e., the number of the beams contributing to  $\mathcal{T}$  can be controlled by a relatively slight variation in  $kL$ . The values of  $\phi_{\pm 1}$  vary from  $\pm 22^\circ$  at  $kL=16.75$  to  $\pm 19.5^\circ$  at  $kL=k_{\pm 3}L=6\pi$ , and those of  $\phi_{\pm 2}$  do from  $\pm 50.9^\circ$  at  $kL=16.2$  to  $\pm 41.8^\circ$  at  $kL=6\pi$ .

In Fig. 11, IFCs are presented for the two peculiar  $kL$  ranges from Fig. 10, within which unidirectional translation takes place. Since the IFCs are located at  $k=\hat{k}$  around  $M$  point, construction lines should be drawn by taking into account only the periodicity of the front-side interface. In Fig.

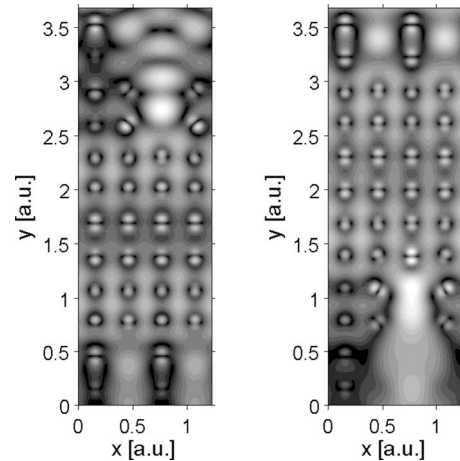


FIG. 9. Electric field pattern at  $0 < x < L$ ,  $0 < y < Pa$ , and  $kL=15$  in CUL case (left) and CLU case (right) from Fig. 8.

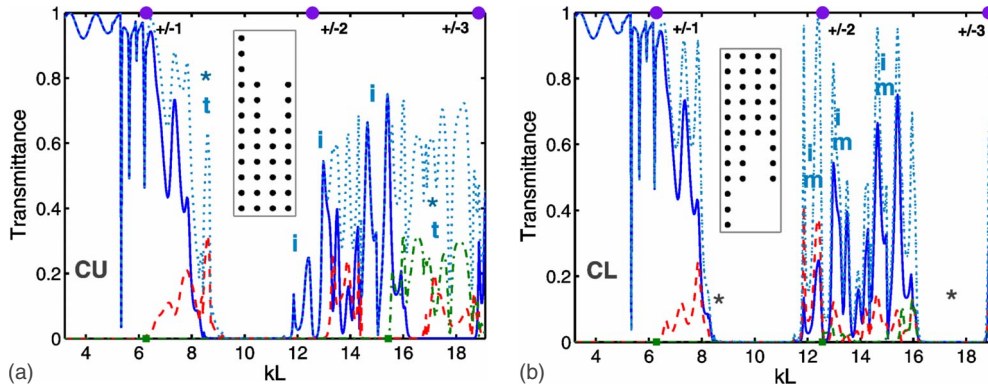


FIG. 10. (Color online) Same as Figs. 2(a) and 2(c) but for  $\epsilon_r=5.8$ .

11(a), only the orders with  $n = \pm 1$  are coupled to a FB wave at  $k = \hat{k}$  in the CU case due to the hyperbolic-type IFCs. No coupling is expected to appear in the corresponding CL case. These features are similar to those in Figs. 2 and 5(a) at  $kL \approx 6.5$ . The only difference is that the ranges of  $\mathcal{T}^{\text{CU}} = t_0 + t_{-1} + t_{+1}$  and  $\mathcal{T}^{\text{CU}} = t_{-1} + t_{+1}$  are adjacent in Fig. 10(a), instead of the ranges of  $\mathcal{T}^{\text{CU}} = t_0$  and  $\mathcal{T}^{\text{CU}} = t_{-1} + t_{+1}$  in Fig. 2(a). Transformation of the IFC shape into that associated with an isotropic media with  $N_{\text{eff}} > 1$  occurs at decreasing  $kL$ , e.g., at  $kL = 8.1$  in Fig. 11(a). This leads to that the translation becomes bidirectional, as seen from the comparison of Figs. 10(a) and 10(b). Therefore, translation can be tuned from bidirectional to unidirectional by a slight variation in  $kL$ .

In Fig. 11(b), the IFCs are shown for the  $kL$  values corresponding to the lower edge of and inside a wide range of unidirectional transmission, which appears at  $16.25 < kL < 18.7$ , see Fig. 10(a). In contrast to Fig. 7, the negative refraction occurs here for the transmission channels with  $n = \pm 1$  at the back-side interface in CU case, i.e.,  $\text{sgn}(\mathbf{v}_g \cdot \mathbf{x}) \neq \text{sgn}(\mathbf{k}_n \cdot \mathbf{x})$ . These channels mimic refraction at a virtual flat front-side interface at  $\theta \neq 0$ . For the two other channels ( $n = \pm 2$ ), collimation and propagation in the PC in normal direction with respect to the noncorrugated back-side interface and deflection of the transmitted beam at this interface take place. Note that the effective photonic mass is positive at the corner of the FBZ for the third FB wave so that  $\mathbf{S} \cdot \mathbf{k}^{\text{PC}} < 0$  without an effective-index behavior. The mass remains positive while the IFCs are narrowing at decreasing  $kL$ , leading to that only the orders with  $n \pm 2$  contribute to  $\mathcal{T}^{\text{CU}}$  for  $16.25 < kL < 16.73$ .

Based on the presented results, a *condition of multibeam unidirectionality* that involves the deflected beams with different  $|n| > 0$  can be written at  $ka < 2\pi$  as follows:

$$k_{\text{min},x}^{\text{PC}} < |k \sin \phi_{\pm n}| < 2\pi - k_{\text{min},x}^{\text{PC}}, \quad (19)$$

where  $k_{\text{min},x}^{\text{PC}} > 0$ , at least for two pairs of the higher orders  $\pm n$ .

### E. Oblique incidence

Let consider some peculiarities of diffraction at nonzero  $\theta$ . It can be shown that taking PC with IFCs, which are associated with the isolation regime at  $\theta = 0$ , one can substantially modify the contribution of individual orders to  $\mathcal{T}$ . Furthermore, the old (zero-order) channel can be closed while new ones are opening. Two examples are shown in Fig. 12, which demonstrate typical features of  $t_n$  vs  $kL$  within the  $kL$  ranges being adjacent to the lowest band gap. In particular, the order with  $n = -1$  dominates at  $4 < kL < 6$ . In the CU case, this is the sole order that contributes to  $\mathcal{T}$  at  $kL = 11$ . In the comparison with Fig. 2(a), the orders with  $n = 0$  and  $|n| = 1$  interchange their roles at the upper edge of the gap. While  $\phi_{-1}$  is varied from  $-59.7^\circ$  at  $kL = 4$  to  $-19.9^\circ$  at  $kL = 6$ , and from  $6.7^\circ$  at  $kL = 10.65$  to  $9^\circ$  at  $kL = 11.4$ , the various deflection regimes can be obtained. In the former case, birefringence appears so that the dominant first-negative-order beam is negatively deflected ( $\phi_{-1} < 0$ ). In the latter case, the first-negative-order beam is positively deflected ( $\phi_{-1} > 0$ ).

In Fig. 12,  $\mathcal{T}^{\text{CL}} = 0$  and  $\mathcal{T}^{\text{CU}} \approx 0.805$  at  $kL = 11.007$ . Now unidirectionality is realized due to a sole order, which trans-

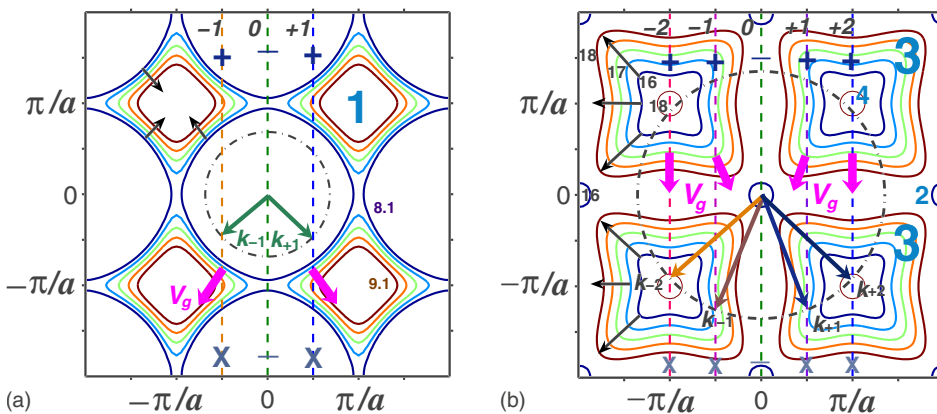


FIG. 11. (Color online) IFCs for PC with  $d/a = 0.4$ ,  $\epsilon_r = 5.8$ , and  $ml = 4$ ;  $kL = 8.1, 8.35, 8.6, 8.85$ , and  $9.1$  in case (a);  $kL = 16, 16.5, 17, 17.5$ , and  $18$  in case (b); directions of  $\mathbf{k}_n$  and  $\mathbf{v}_g$  in CU case, and IFC in air are shown at (a)  $kL = \hat{k}L = 7.5$  and (b)  $17$ ; notations are the same as in Fig. 3.

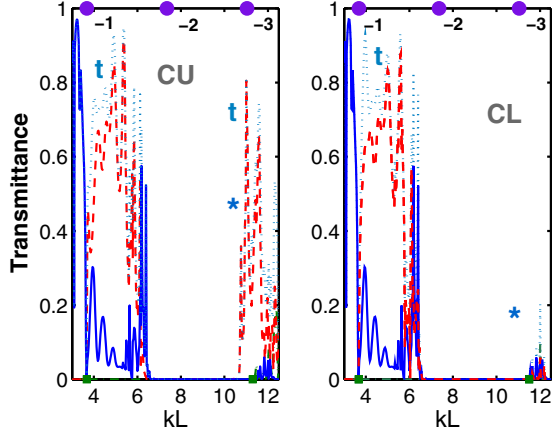


FIG. 12. (Color online) Transmittance for PC grating with the same parameters as in Fig. 2(a) (left plot) and Fig. 2(c) (right plot), respectively, except for  $\theta = \pi/4$ ; notations are the same as in Fig. 2.

fers even a bigger part of the incident-wave energy than in the previous examples. Therefore, IFCs located around  $M$  point are not necessary. This effect can be considered as the extrinsically achievable unidirectionality since it appears at  $\theta \neq 0$  and is absent at  $\theta = 0$ . In terms of the appearance conditions, it is similar to the effect of the extrinsic chirality, which can appear in some metamaterials while taking  $\theta \neq 0$  instead of  $\theta = 0$ .<sup>48</sup> Note that the order with  $n = -3$  may contribute to  $\mathcal{T}$  according to Eq. (8) at  $k > k_{\pm 3}L = 11.04$ . Its effect is not considered here.

Figure 13 shows IFCs and directions of  $\mathbf{k}_n$  and  $\mathbf{v}_g$ , which correspond to the two peculiar  $kL$  ranges from Fig. 12. In Fig. 13(a), the both propagating orders are coupled to the first FB wave at  $k = \hat{k}$ . Here,  $|k \sin \phi_{-1}| < k_{\max,x}^{\text{PC}}$ ,  $|k \sin \phi_{-2}| > k_{\max,x}^{\text{PC}}$ ,  $|k \sin \phi_{+1}| > k_{\max,x}^{\text{PC}}$ , and  $|k \sin \theta| < k_{\max,x}^{\text{PC}}$ . The open transmission channels are associated with different sign of refraction at a virtual flat front-side interface,  $\text{sgn}(\mathbf{k}_0 \cdot \mathbf{x}) \neq \text{sgn}(\mathbf{k}_{-1} \cdot \mathbf{x})$  while  $\mathbf{S} \cdot \mathbf{k}^{\text{PC}} > 0$ . Comparing to Fig. 12(a), one can see that the channel at  $n = -1$ , that corresponds to  $\mathbf{k}_{-1} \cdot \mathbf{x} < 0$ , is coupled to the negatively deflected transmitted beam ( $\phi_{-1} < 0$ ), providing the dominant contribution to  $\mathcal{T}$  at  $4 < kL < 6$ . Since the IFCs correspond here to an isotropic medium with  $N_{\text{eff}} \approx 1.68$ , the bidirectional translation occurs so that the both channels remain open regardless of whether CU or CL case is considered. Similar situation occurs in Fig. 10 at least at  $2\pi < kL < 8.5$ .

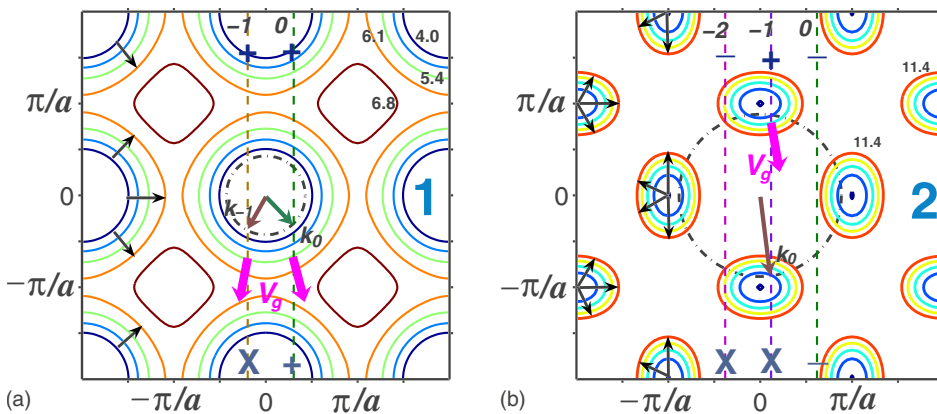


FIG. 13. (Color online) IFCs for PC at  $d/a = 0.4$ ,  $\epsilon_r = 11.4$ , and  $ml = 4$ ;  $kL = 4, 4.7, 5.4, 6.1$ , and  $6.8$  in case (a);  $kL = 10.6, 10.8, 11, 11.2$ , and  $11.4$  in case (b); directions of  $\mathbf{k}_n$  and  $\mathbf{v}_g$  in CU case and IFC in air are shown at (a)  $kL = \hat{k}L = 5.4$  and (b) 11; construction lines are shown for  $\theta = \pi/4$ ; remaining notations are the same as in Fig. 3.

The fundamental difference between the cases in Figs. 13(a) and 13(b) is that the IFCs in PC are wider and narrower than in air, respectively. In turn, zero order can be uncoupled to a FB wave in the latter case but is always coupled in the former case. In Fig. 13(b),  $\mathbf{S} \cdot \mathbf{k}^{\text{PC}} < 0$ ,  $k_{\max,x}^{\text{PC},1} < |k \sin \phi_0| < k_{\min,x}^{\text{PC},2}$ ,  $k_{\max,x}^{\text{PC},1} < |k \sin \phi_{-2}| < k_{\min,x}^{\text{PC},2}$ , and  $|k \sin \phi_{-1}| < k_{\max,x}^{\text{PC},1}$ , where the indices 1 and 2 stand for the groups of IFCs, which are located around the points with the abscissa values  $k_x = 0$  and  $k_x = \pi/a$ , respectively.

Construction lines are plotted in Fig. 13(b) in CU and CL cases according to the above formulated rule for anisotropic-like IFCs. Then, no order is coupled to the second FB wave in CL case while one order is coupled in CU case. This is in agreement with the transmission results in Fig. 12. It is noteworthy that the unidirectionality is not necessarily connected with a transmission channel, which corresponds to a positive refraction, as in Fig. 13(b). For example, the sole transmission channel in case of IFCs shown in Fig. 13(b) would be associated with negative refraction if

$$\sin^{-1}(k_{\max,x}^{\text{PC},1}/k) < \theta < \sin^{-1}(2\pi/kL).$$

In particular, it occurs for  $k = \hat{k}$  nearly at  $21^\circ < \theta < 34.8^\circ$ . Besides, the situation when

$$\phi_0(\theta_1) = \phi_{-1}(\theta_2)$$

and hence  $\mathbf{k}_0(\theta_1) = \mathbf{k}_{-1}(\theta_2)$  can be realized for a sole transmitted beam, where  $\theta_1$  and  $\theta_2$  are two angles of incidence,  $\theta_1 \neq \theta_2$ .

Another effect connected with the IFCs being narrower than in air is schematically illustrated in Fig. 14. It corresponds to a special case when the sole transmitted higher-order beam mimicks that with  $n = 0$  at  $\theta = 0$  in the isolation regime. Setting  $\phi_n = 0$  in Eq. (10), we obtain the condition

$$kL \sin \theta = -2\pi n, \quad (20)$$

at which this regime is realized, provided that there is a sole propagating order  $n$  being coupled to a FB wave. A transmitted  $n$ th-order beam is negatively deflected at  $\theta > 0$  ( $\phi_n < 0$ ), whatever the IFCs are, if

$$kL \sin \theta + 2\pi n < 0. \quad (21)$$

The conditions of existence of the isolation and translation regimes can be obtained for nonzero  $\theta$ , which are similar to those given for  $\theta = 0$  in Sec. III B. Very recently, it has been

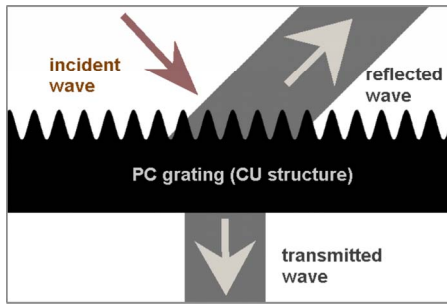


FIG. 14. (Color online) A special case of deflection when transmitted wave propagates in normal direction.

shown that unidirectionality can also be realized at  $\theta \neq 0$  for the gratings, which contain ultralow-index flat layers that are characterized by isotropic IFCs being narrower than those in air.<sup>49</sup> Hence, the presence of anisotropic-like IFCs should be considered rather as a sufficient condition of unidirectionality than a necessary one.

#### IV. CONCLUSIONS

To summarize, the anomalous one-way transmission effects arising in diffraction on nonsymmetric PC gratings with one- and two-side corrugations have been studied and classified. In particular, they manifest themselves in that one or several diffraction orders can significantly contribute to the transmitted far field, if the PC grating with different periods at the front- and back-side interfaces is illuminated from one side and do not contribute at all at the same illumination from the other side. Furthermore, the situation can be realized for the grating illuminated from the side of the noncorrugated interface, when all the propagating orders are totally reflected so that unidirectional transmission does appear. For the opposite-side illumination, more than 80 and 70 percent of the incident-wave energy can be transmitted in the single beam and multibeam regimes, respectively. Hence, unidirectionality can be achieved within the reciprocal framework, showing an alternative route to that requiring the use of anisotropic constituents. In our case, it is connected with the possibility of existence of anisotropic-like IFCs in PCs, which are made of isotropic materials, and the relevant peculiarities of the transmission channels. Polarization of the waves involved to the diffraction always remains linear that differs from the anisotropic framework.

In terms of the effect exerted by the front-side corrugations on the transmitted field, translation and isolation regimes can be distinguished. In turn, the unidirectionality is associated with one of the two cases assigned to the transla-

tion regime, for which the necessary condition is that zero order is not coupled to a FB wave. Instead, the parallel (tangential) component of the wave vector for one or several higher orders arising due to the corrugations should be equal to that of a FB wave. In the isolation regime, the back-side corrugated interface can modify the transmitted field in such a way that the contribution of higher orders is significant while not all of them are coupled to a FB wave. Hence, transmission features originating from the intrinsic properties of PC can be masked by the diffraction. The duality can appear in that the same orders do not contribute to the transmission in CU case and to the reflection in the corresponding CL case within some frequency ranges.

It has been demonstrated how construction lines should be plotted, depending on the IFC topology, and which information can be inferred from the wave-vector diagrams. In particular, the existence of translation, isolation, and unidirectionality can be predicted. In contrast to the topology, the handedness is not critical for obtaining of these regimes. In some cases, anomalous transmission effects, including unidirectionality, cannot be predicted using IFCs and wave-vector diagrams. They might be related to the existence of preferable conditions for certain transmission channels in PC and to the fact that the PC layers corresponding to corrugations can themselves represent a lattice, which is different from that of a regular part of PC grating.

A variety of theoretical performances, in which unidirectionality is obtainable, can be extended due to using nonzero angle between the  $\Gamma$ -X direction of PC and the noncorrugated back-side interface. The isolation and translation can coexist in the same structure at the same frequency, within adjacent ranges of variation in the angle of incidence. Besides, one should mention the possibility of engineering multibeam systems with desired combinations of the positively and negatively refracted/deflected beams. Although obtaining of a reflection-free unidirectionality in PC gratings still seems to be a challenging task, such structures with different periods at the front and back sides look promising for realization of an alternative approach to the achieving of unidirectionality. Analysis of the possibilities of obtaining a reflection-free unidirectional transmission owing to optimization of the gratings based on PCs with anisotropic-like IFCs and unidirectionality in the gratings based on PCs with isotropic IFCs are under study.

#### ACKNOWLEDGMENT

The author would like to thank the Deutsche Forschungsgemeinschaft for partial support of this work under the Project No. SE1409.2-1.

\*serebryannikov@tu-harburg.de

<sup>1</sup>P. Vodo, P. V. Parimi, W. T. Lu, and S. Sridhar, *Appl. Phys. Lett.* **86**, 201108 (2005).

<sup>2</sup>F. Abdel Malek, W. Belhadj, S. Haxha, and H. Bouchriha, *J.*

*Lightwave Technol.* **25**, 3168 (2007).

<sup>3</sup>B. Gralak, S. Enoch, and G. Tayeb, *J. Opt. Soc. Am. A* **17**, 1012 (2000).

<sup>4</sup>Y. Saado, M. Golosovsky, A. Davidov, and A. Frenkel, *J. Appl.*

- Phys. **98**, 063105 (2005).
- <sup>5</sup>L. Wu, M. Mazilu, J.-F. Gallet, and T. F. Krauss, Appl. Phys. Lett. **86**, 211106 (2005).
- <sup>6</sup>J. Zarbakhsh, F. Hagmann, S. F. Mingaleev, K. Busch, and K. Hingerl, Appl. Phys. Lett. **84**, 4687 (2004).
- <sup>7</sup>S. Nojima, J. Opt. A, Pure Appl. Opt. **9**, S425 (2007).
- <sup>8</sup>G. Colas des Francs, C. Girard, J.-C. Weeber, C. Chicane, T. David, A. Dereux, and D. Peyrade, Phys. Rev. Lett. **86**, 4950 (2001).
- <sup>9</sup>J. Scheuer and A. Yariv, Phys. Rev. E **70**, 036603 (2004).
- <sup>10</sup>D. P. Gaillot, C. Croenne, and D. Lippens, Opt. Express **16**, 3986 (2008).
- <sup>11</sup>D. Xiao and H. T. Johnson, Opt. Lett. **33**, 860 (2008).
- <sup>12</sup>Y. Huang, Y. Feng, and T. Jiang, Opt. Express **15**, 11133 (2007).
- <sup>13</sup>S. K. Morrison and Y. S. Kivshar, Appl. Phys. Lett. **86**, 081110 (2005).
- <sup>14</sup>R. Moussa, B. Wang, G. Tuttle, Th. Koschny, and C. M. Soukoulis, Phys. Rev. B **76**, 235417 (2007).
- <sup>15</sup>W. Smigaj, Phys. Rev. B **75**, 205430 (2007).
- <sup>16</sup>H. Caglayan, I. Bulu, and E. Ozbay, J. Appl. Phys. **104**, 073108 (2008).
- <sup>17</sup>Z.-H. Zhu, W.-M. Ye, J.-R. Ji, X.-D. Yuan, and C. Zen, Appl. Phys. B **86**, 327 (2007).
- <sup>18</sup>S. Collardey, A.-C. Tarot, P. Pouliguen, and K. Mahdjoubi, Microwave Opt. Technol. Lett. **44**, 546 (2005).
- <sup>19</sup>A. E. Serebryannikov, T. Magath, and K. Schuenemann, Phys. Rev. E **74**, 066607 (2006).
- <sup>20</sup>The term “nonordinary” instead of “extraordinary” has been used to underline the difference between the effects considered and those known as extraordinary for anisotropic media.
- <sup>21</sup>W. T. Lu, Y. J. Huang, P. Vodo, R. K. Banyal, C. H. Perry, and S. Sridhar, Opt. Express **15**, 9166 (2007).
- <sup>22</sup>M. J. Lockyear, A. P. Hibbins, K. R. White, and J. R. Sambles, Phys. Rev. E **74**, 056611 (2006).
- <sup>23</sup>Z. Wang, Y. D. Chong, J. D. Joannopoulos, and M. Soljacic, Phys. Rev. Lett. **100**, 013905 (2008).
- <sup>24</sup>F. D. M. Haldane and S. Raghu, Phys. Rev. Lett. **100**, 013904 (2008).
- <sup>25</sup>A. Figotin and I. Vitebskiy, Phys. Rev. B **67**, 165210 (2003).
- <sup>26</sup>A. Figotin and I. Vitebskiy, J. Magn. Mater. **300**, 117 (2006).
- <sup>27</sup>R. A. Depine and A. Lakhtakia, Phys. Rev. E **69**, 057602 (2004).
- <sup>28</sup>R. A. Depine, A. Lakhtakia, and D. R. Smith, Phys. Lett. A **337**, 155 (2005).
- <sup>29</sup>R. A. Depine, M. E. Inchaussandague, and A. Lakhtakia, J. Opt. Soc. Am. B **23**, 514 (2006).
- <sup>30</sup>A. E. Serebryannikov, T. Magath, K. Schuenemann, and O. Y. Vasylchenko, Phys. Rev. B **73**, 115111 (2006).
- <sup>31</sup>M. McCall and A. Lakhtakia, Electromagnetics **23**, 1 (2003).
- <sup>32</sup>J. P. McIlroy, M. W. McCall, A. Lakhtakia, and I. J. Hodgkinson, Optik (Stuttgart) **116**, 311 (2005).
- <sup>33</sup>V. Fiumara, F. Chiadini, A. Scaglione, and A. Lakhtakia, Opt. Commun. **268**, 182 (2006).
- <sup>34</sup>N. Le Thomas, R. Houdré, L. H. Frandsen, J. Fage-Pedersen, A. V. Lavrinenko, and P. I. Borel, Phys. Rev. B **76**, 035103 (2007).
- <sup>35</sup>T. Magath and A. E. Serebryannikov, J. Opt. Soc. Am. A **22**, 2405 (2005).
- <sup>36</sup>See, www.cst.com
- <sup>37</sup>B. T. Schwartz and R. Piestun, J. Opt. Soc. Am. B **20**, 2448 (2003).
- <sup>38</sup>M. Silveirinha and N. Engheta, Phys. Rev. B **75**, 075119 (2007).
- <sup>39</sup>A. Alù, M. G. Silveirinha, A. Salandrino, and N. Engheta, Phys. Rev. B **75**, 155410 (2007).
- <sup>40</sup>K. Guven, K. Aydin, K. B. Alici, C. M. Soukoulis, and E. Ozbay, Phys. Rev. B **70**, 205125 (2004).
- <sup>41</sup>S. Foteinopoulou and C. M. Soukoulis, Phys. Rev. B **72**, 165112 (2005).
- <sup>42</sup>*Electromagnetic Theory of Gratings*, edited by R. Petit (Springer, Berlin, New York, 1980).
- <sup>43</sup>T. Baba and M. Nakamura, IEEE J. Quantum Electron. **38**, 909 (2002).
- <sup>44</sup>S. Enoch, G. Tayeb, P. Sabouroux, N. Guerin, and P. Vincent, Phys. Rev. Lett. **89**, 213902 (2002).
- <sup>45</sup>C. Luo, S. G. Johnson, J. D. Joannopoulos, and J. B. Pendry, Phys. Rev. B **65**, 201104(R) (2002).
- <sup>46</sup>The energy velocity is equal to the group velocity in PCs, e.g., see Ref. 41. On the other hand,  $\mathbf{v}_e = \langle \mathbf{S} \rangle / \langle U \rangle$ , where  $\mathbf{S}$  and  $U$  mean the Poynting vector and the energy density.
- <sup>47</sup>In the contrast to homogeneous media, the IFC are periodic in our case. Therefore, the IFCs that are located around a periphery point of the FBZ are referred to as anisotropiclike IFCs, or hyperbolic-type IFCs, while keeping in mind that this analogy is valid only if  $k_x < |\pi/a|$  and  $k_y < |\pi/a|$  and that the symmetries are different.
- <sup>48</sup>E. Plum, V. A. Fedotov, and N. I. Zheludev, Appl. Phys. Lett. **93**, 191911 (2008).
- <sup>49</sup>A. E. Serebryannikov and E. Ozbay, Opt. Express **17**, 13335 (2009).